Martian low-altitude magnetic topology deduced from MAVEN/SWEA observations

Shaosui Xu, David Mitchell, Michael Liemohn, Xiaohua Fang, Yingjuan Ma, Janet Luhmann, David Brain, Morgane Steckiewicz, Christian Mazelle, Jack Connerney, et al.

AGU PUBLICATIONS

JGR

Journal of Geophysical Research: Space Physics

RESEARCH ARTICLE
10.1002/2016JA023373

Key Points:
- An event with both CDPS and SDPS observations is reproduced in an OpenGGCM simulation
- CDPS is the main source of SDPS in its early stage
- CDPS and a subsequent IMF southward turning causes the formation of SDPS

Correspondence to:
W.-H. Li,
WenhuiLi88@yahoo.com

Citation:
Li, W.-H., J. Raeder, M. F. Thomsen, B. Lavraud, L.-Z. Lü, and E.-W. Liang (2017), The formation of superdense plasma sheet in association with the IMF turning from northward to southward, *J. Geophys. Res. Space Physics*, *122*, 2936–2955, doi:10.1002/2016JA023373.

Received 23 AUG 2016
Accepted 29 JAN 2017
Accepted article online 1 FEB 2017
Published online 7 MAR 2017

The formation of superdense plasma sheet in association with the IMF turning from northward to southward

Wen-Hui Li[1], Joachim Raeder[2], Michelle F. Thomsen[3], Benoit Lavraud[4], Lian-Zhong Lü[1], and En-Wei Liang[1]

[1] Astrophysics and Space Science Center, Guangxi University, Nanning, Guangxi, China, [2] Space Science Center, University of New Hampshire, Durham, New Hampshire, USA, [3] Space Science and Applications, Los Alamos National Laboratory, Los Alamos, New Mexico, USA, [4] Institut de Recherche en Astrophysique et Planétologie, Paul Sabatier University, Toulouse, France

Abstract We have studied two events in which relatively superdense plasma appeared near geosynchronous orbit after the interplanetary magnetic field (IMF) changed from a long period of northward condition to southward condition. We used the magnetosphere MHD model Open Geospace General Circulation Model to simulate these two events and compared the simulation results with observations. The observations and the simulation results show that an extended period of northward IMF caused a cold dense plasma sheet (CDPS) to form in the near tail, and a subsequent southward IMF caused a highly stretched near-tail dipole field, which enhanced the earthward convection and eventually set off reconnection. Some of the cold dense plasma was thus consequently transported to geosynchronous orbit and formed a superdense plasma sheet (SDPS). CDPS is the main source of SDPS in its early stage after the IMF southward turning.

1. Introduction

Borovsky et al. [1997] showed that the plasma density of the plasma sheet at geosynchronous orbit was usually in a range of 0.4–2.0 cm^{-3}, and ~6% of the plasma observations showed a density higher than 2.0 cm^{-3}. They considered such plasma as superdense plasma. The ion temperature of the superdense plasma ranges from 5 to 20 keV. The superdense plasma sheet (SDPS) was found to be associated with a particular temporal pattern of *Kp*: *Kp* increasing after it has been low. Near the Earth at the onset of a superdense plasma sheet the density typically rises to very high values (>3 cm^{-3}) and then decays gradually over several hours, although the superdense plasma can flow around the Earth in ~12–18 h [*Borovsky et al.*, 1997, 1998a; *Thomsen et al.*, 2003].

In statistical studies using Los Alamos National Laboratory (LANL) Magnetospheric Plasma Analyzer (MPA) measurements for the period 1990–2004, *Lavraud et al.* [2005, 2006a] reported two distinct cold ($T < 5$ keV), dense ($N > 2$ cm^{-3}) ion populations at geosynchronous orbit. One population was observed in midnight region of geosynchronous orbit. The other population was detected at dawnside of geosynchronous orbit. No such cold, dense population was observed at duskside of geosynchronous orbit on a frequent basis. It was suggested that the source of the midnight population was cold, dense plasma sheet (CDPS), which was often found in the midtail (~10 R_E – ~30 R_E) after several hours of interplanetary magnetic field (IMF) with a positive GSM *z* (northward) component [*Fairfield et al.*, 1981; *Baumjohann et al.*, 1989; *Lennartsson*, 1992; *Fujimoto et al.*, 1996, 1998, 2002; *Terasawa et al.*, 1997; *Phan et al.*, 1998; *Fuselier et al.*, 1999; *Øieroset et al.*, 2002, 2005]. The dawnside cold and dense ion population was associated with previously strong southward IMF and consequently occurs during substantial geomagnetic activity.

In a survey of superdense plasma events observed by MPA instruments, *Thomsen et al.* [2003] found that a superdense plasma sheet would be likely to occur under one of the following two conditions: (1) a sudden southward IMF that follows an extended interval of northward field and (2) a very strong magnetospheric compression caused by a large increase in the solar wind dynamic pressure, also under conditions of northward IMF. They also suggested that, under condition (1), a southward turning of IMF causes the cold dense plasma sheet formed in the midtail during the previous northward IMF period to be pushed toward the geosynchronous orbit.

Borovsky and Steinberg [2006] found that high-speed-stream-driven storms were regularly preceded by a period of calm geomagnetic activity, during which both IMF GSM B_z and IMF GSE B_z were positive on average. SDPS events are also common in the magnetosphere during high-speed-stream-driven storms [*Borovsky et al.*, 1997; *Denton et al.*, 2006]. In some SDPS events, after calms before the storms, cool dense plasma can be seen at geosynchronous orbit after convection commences. This anomalously cool and dense plasma appears sporadically at geosynchronous orbit during the early phase of recurring high-speed-stream-driven storms.

The plasma sheet is an important source for the ring current [*Borovsky et al.*, 1998b; *Jordanova et al.*, 1998; *Kozyra et al.*, 1998; *Thomsen et al.*, 1998; *Ebihara et al.*, 2005]. A cold and dense plasma sheet may lead to a substantially larger ring current [*Lavraud et al.*, 2006a; *Lavraud and Jordanova*, 2007; *Liemohn et al.*, 2008].

Although the statistical data shown by *Thomsen et al.* [2003] and *Lavraud et al.* [2005, 2006a] strongly indicated that the cold dense plasma accumulated in the midtail plasma sheet during northward IMF conditions is the probable source of the superdense plasma observed at geosynchronous orbit, no direct observation involving measurements from the midtail to the near tail and down to the ground altogether has been reported before. Here we report an event that closely relates CDPS and SDPS in association with condition (1) suggested by *Thomsen et al.* [2003]. To further understand the SDPS formation process, we make use of the global magnetosphere MHD model OpenGGCM [*Raeder et al.*, 1998, 2001; *Raeder*, 2003] to simulate this event and an event reported by *Thomsen et al.* [2003] to reveal in detail how plasma may be transported from midtail CDPS to geosynchronous orbit.

2. MHD Model and Simulation

OpenGGCM has been used to simulate a CDPS event with a high degree of agreement with observations [*Li et al.*, 2005; *Øieroset et al.*, 2005]. It also successfully simulated a cold dense magnetopause boundary layer observed by THEMIS under northward IMF condition [*Li et al.*, 2009; *Øieroset et al.*, 2008]. It has been used to studied solar wind entry into the magnetosphere under northward IMF condition [*Li et al.*, 2008]. Therefore, OpenGGCM is an appropriate tool to study the formation of SDPS in relation to CDPS.

OpenGGCM solves the resistive MHD equations on a nonuniform rectilinear grid where the minimum grid space *dy* (*dz*) locates at GSE $y = 0$ ($z = 0$) and the minimum *dx* locates at a point near the magnetopause standoff distance while the maximum grid space is at the outer boundary. The outer boundary conditions on the dayside are the solar wind and IMF conditions, while those on the other five outer boundaries are free (i.e., normal derivatives vanish). The inner boundary conditions are derived from the coupling with an ionospheric model. Field-aligned currents are computed just outside a spherical region of radius 3.5 R_E and mapped to a spherical-polar ionosphere grid at 1 R_E using a dipole magnetic field model. The ionosphere potential is solved on the surface of a sphere with 1.02 R_E radius. The ionospheric electric field is mapped back to the surface of the sphere with 3.5 R_E radius. In an OpenGGCM simulation, the ionosphere can be either simply set to be a sphere with constant uniform conductance, modeled by empirical parameters [*Robinson et al.*, 1987] or modeled by the NOAA Coupled Thermosphere Ionosphere Model (CTIM) [*Fuller-Rowell et al.*, 1996]. A more detailed description of the OpenGGCM model and its ionosphere coupling can be found in related articles [*Raeder et al.*, 1998, 2001; *Raeder*, 2003; *Raeder et al.*, 2008].

For this simulation study, we used solar wind data from ACE spacecraft to drive the simulation in a domain of $(-600, 25) \times (-45, 45) \times (-45, 45) R_E$ in GSE coordinates. The grid has $480(x) \times 250(y) \times 250(z)$ points and a minimum grid spacing of 0.2 R_E near the dayside magnetopause region. CTIM was used as the coupled ionosphere model. During the first half hour, the IMF was manually set to be southward so that an ordinary magnetosphere could be formed quickly. The geomagnetic dipole was fixed at the orientation corresponding to the moment when the IMF was turning from northward to southward at the magnetopause. The magnetosphere values of the whole domain were written out every 6 min, and the same set of values on certain two-dimensional cut planes was written out every 2 min. The values at a given position and a given time can be obtained from linear spatial and temporal interpolation for further analysis and tracing of fluid elements. The version of OpenGGCM used in this simulation study does not include any inner magnetosphere model.

3. Event on 14 September 2001

This event has relevant observations at several locations such as the ACE satellite, the Wind satellite, the Cluster satellites, the LANL satellites, the NASA Imager for Magnetopause-to-Aurora Global Exploration (NASA IMAGE)

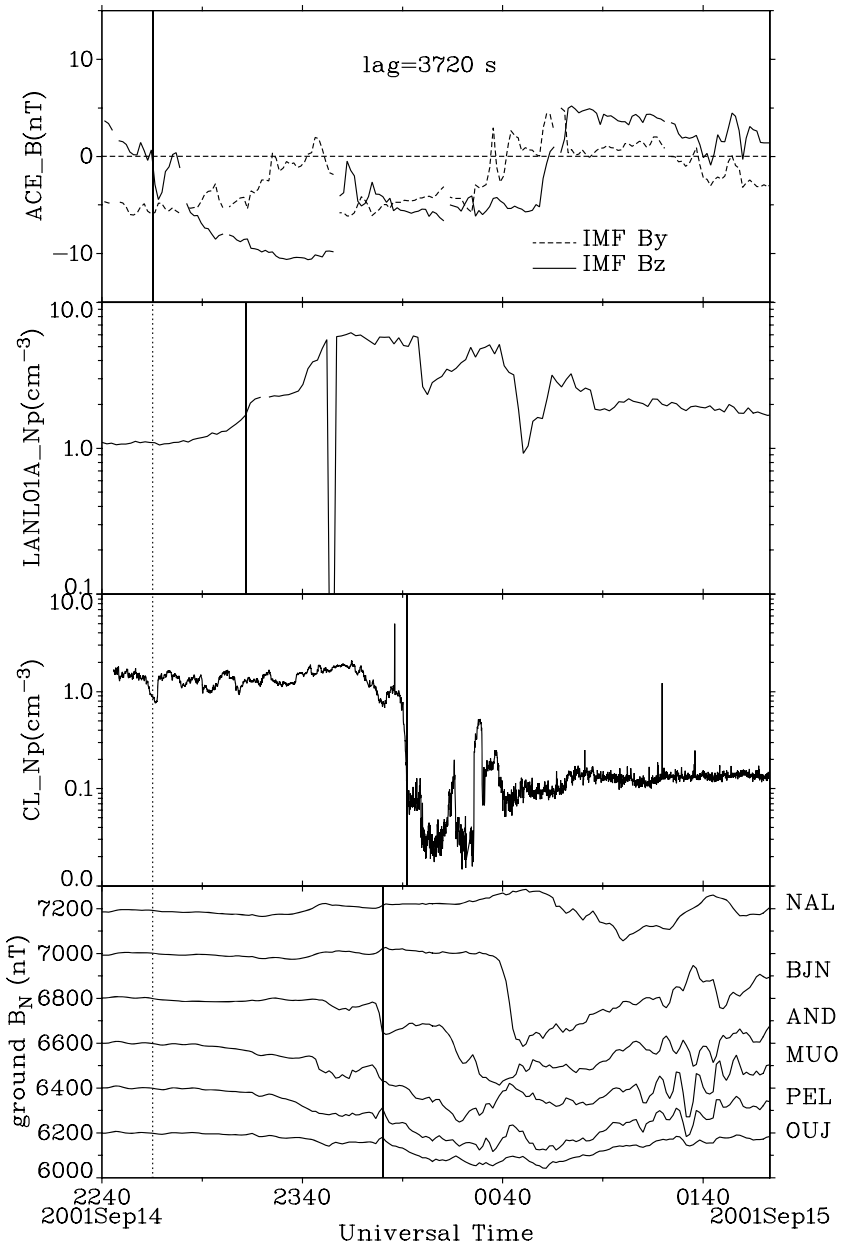

Figure 1. Overview of the SDPS event from 22:40 UT on 14 September 2001 to 02:00 UT on 15 September 2001. Shown from top to bottom are shifted IMF *y* and *z* components measured at ACE, proton number density measured by LANL01A MPA instrument, plasma density measured by Cluster, and the northern component of the ground magnetic field measured by ground stations. The solid vertical lines from top to bottom indicate the IMF southward turning at magnetopause, the arrival of SDPS at geosynchronous orbit, the disappearance of CDPS at Cluster, and the beginning of ground magnetic field disturbance, respectively.

spacecraft, and the International Monitor for Aurora Geomagnetic Effects (IMAGE) magnetometer network stations. In this section, we will show the observations on these locations and some corresponding simulation results.

3.1. Event Overview

Figure 1 summarizes this event with observations from several locations. After ~20 h of strong northward IMF, the southward IMF arrived at the magnetopause at ~22:54:00 UT on 14 September 2001. The Magnetospheric Plasma Analyzer instrument on LANL01A spacecraft observed the arrival of superdense plasma at ~23:22:00 UT. Before the arrival of southward IMF, a CDPS had been at the Cluster location for some time.

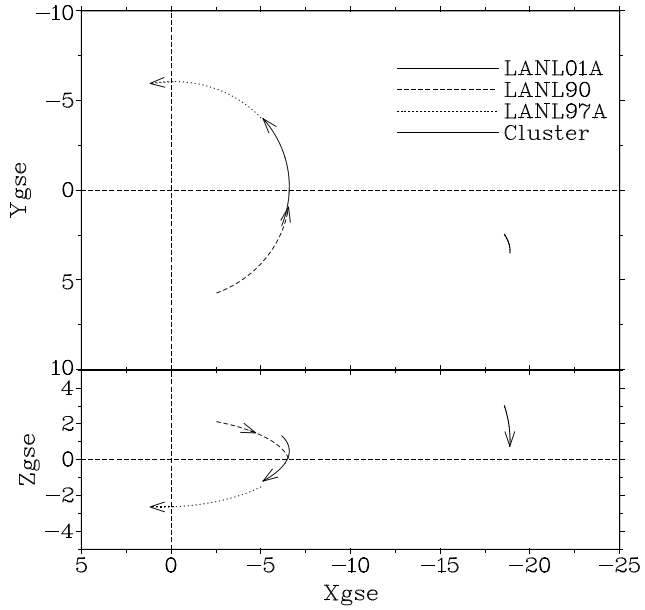

Figure 2. The orbits of the satellites LANL01A, LANL90, LANL97A, and Cluster-1 from 14 22:00:00 UT to 15 02:00:00 UT in September 2001.

The observed CDPS changed into a hot tenuous plasma sheet at 00:10:00 UT the next day, about 1 h and 16 min after the arrival of the southward IMF. The NASA IMAGE spacecraft recorded an auroral substorm event at 23:52:24 UT on 14 September 2001 (not shown here). Ground magnetometers observed a disturbance of northward magnetic field component beginning at ~00:03:00 UT and detected the maximum disturbance at ~00:40:00 UT the next day. During this disturbing time period, the magnetometer stations were near the midnight region.

Figure 2 shows the orbits of LANL satellites and Cluster-1 spacecraft during this event. From ~22:40:00 UT on 14 September to ~02:00:00 UT on 15 September, LANL97A spacecraft was on the dawnside range from ~03:00:00 LT to ~07:00:00 LT, and LANL90 spacecraft was on the duskside range from ~20:00:00 LT to ~24:00:00 LT. LANL01A spacecraft was near the noon-midnight meridian range from ~23:00:00 LT to ~02:30:00 LT. All the LANL satellites were near the GSE equatorial plane on geosynchronous orbit. Cluster spacecraft were ~20 R_E in the tail and were near both the equatorial plane and the noon-midnight meridian.

3.2. Solar Wind Conditions

Figure 3 shows the solar wind and IMF conditions measured by ACE spacecraft. On 14 September 2001, ACE observed a long period (~20 h) of northward IMF followed by a southward turning at ~21:52 UT. The southward IMF arrived at the magnetopause approximately at ~22:54 UT with a traveling time of ~3720 s from the ACE location. The arrival time at the magnetopause was estimated using data from Wind spacecraft. Wind spacecraft was fortuitously located at GSE (51.2, −42.7, 3.7) R_E at 22:45:00 UT and observed the southward IMF turning at this time. It also observed the long period of northward IMF before the southward IMF arrival. The solar wind at ACE was correlated with the solar wind at Wind during this event. This southward IMF lasted for ~2.4 h. During this period of southward IMF, the solar wind speed was ~460 km/s, and the plasma number density variated from ~7 cm^{-3} to ~25 cm^{-3}.

3.3. Cluster Observations

Cluster observations are shown in Figure 4. On 14 September Cluster had no data before 22:40 UT. Cluster Hot Ion Analyzer instrument observed cold dense plasma from 22:40 UT on 14 September to 00:10 UT on 15 September. At 00:10 UT on 15 September, which was ~76 min after the IMF southward turning, Cluster detected a rapid change of plasma density from dense (1.0 cm^{-3}) to tenuous (0.1 cm^{-3}). The temperature changed from 1.0 keV to 9.0 keV gradually with fluctuation from 00:10:00 UT to 00:40:00 UT. These changes suggest that the CDPS was changing into a hot tenuous plasma sheet at the Cluster location. During this period, Cluster observed a highly stretched and building-up magnetic field which suggested that Cluster

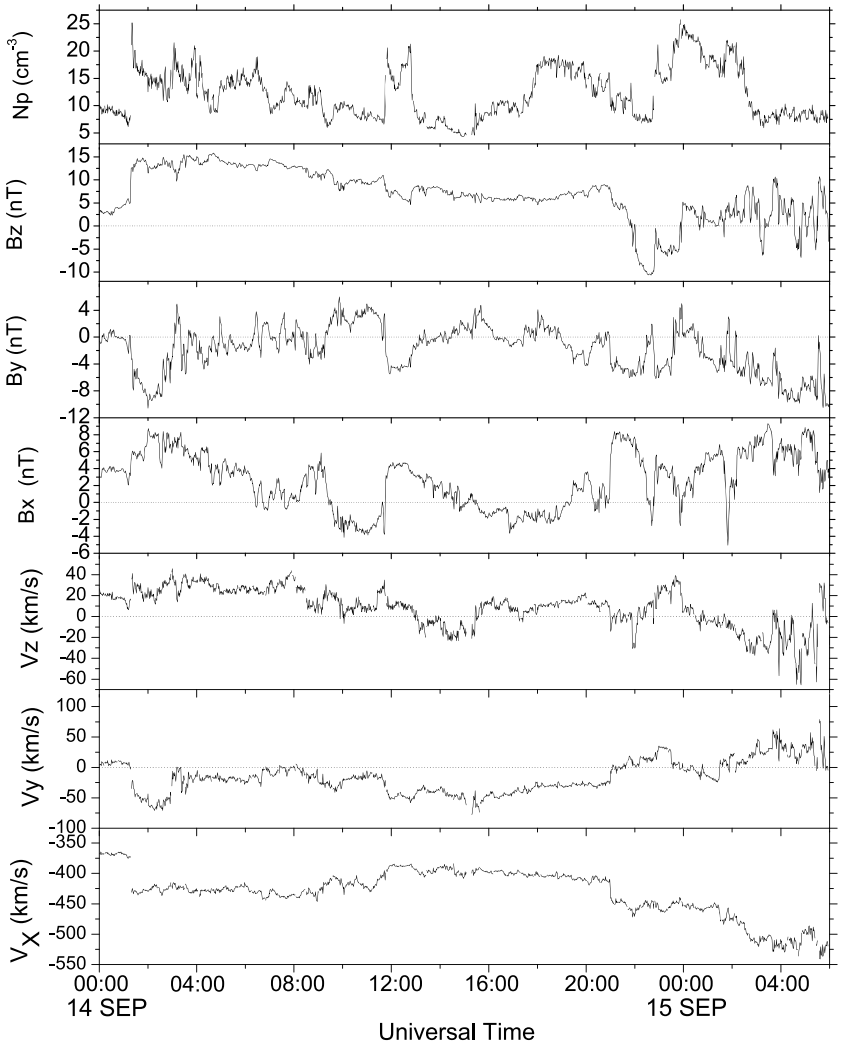

Figure 3. Solar wind conditions at ACE location from 00:00 UT on 14 September 2001 to 06:00 UT on 15 September 2001. Shown properties from top to bottom are plasma number density, IMF components, and solar wind velocity components, all in GSE coordinates.

observed a substorm growth phase from ~23:00 UT to ~00:15 UT the next day. The substorm onset occurred around ~00:15 UT. Shortly after the CDPS disappeared, several bursts of sunward hot plasma flows with speed up to 800 km/s were observed at Cluster from 00:25:00 UT to 00:50:00 UT on 15 September. These flows were most likely bursty bulk flows in the plasma sheet [*Angelopoulos et al.*, 1992]. The magnetic field was then dipolized immediately after the passing of the plasma flow bursts. During this event, the plasma flow was stagnant except the time when the bursty bulk flows were observed.

3.4. Observations at Nightside Geosynchronous Orbit

During this event, three LANL satellites were well positioned in the nightside for the observation of a coming SDPS. As shown in Figure 2, one satellite was near midnight, another one was in dawnside, and the third one was in duskside. Figure 5 shows the observations at geosynchronous orbit. At ~23:22 UT, which was ~28 min after the IMF southward turning at the magnetopause, LANL01A first detected high-density (>2 cm^{-3}) plasma near local midnight position. At ~23:40 UT, LANL97A and LANL90 began to detect similar plasma material at dawnside and duskside, respectively. The plasma then became superdense and much colder for ~40 min. During this period of superhigh-density plasma, the magnetic field at 6.6 R_E in nightside was highly stretched, as indicated by the magnetic field elevation angle (θ), and the convection of plasma was enhanced toward the Earth. The dawnside superdense plasma at LANL97A was transported slightly dawnward, while the dusk-side one at LANL90 was transported significantly duskward, as indicated by the *y* component of the plasma

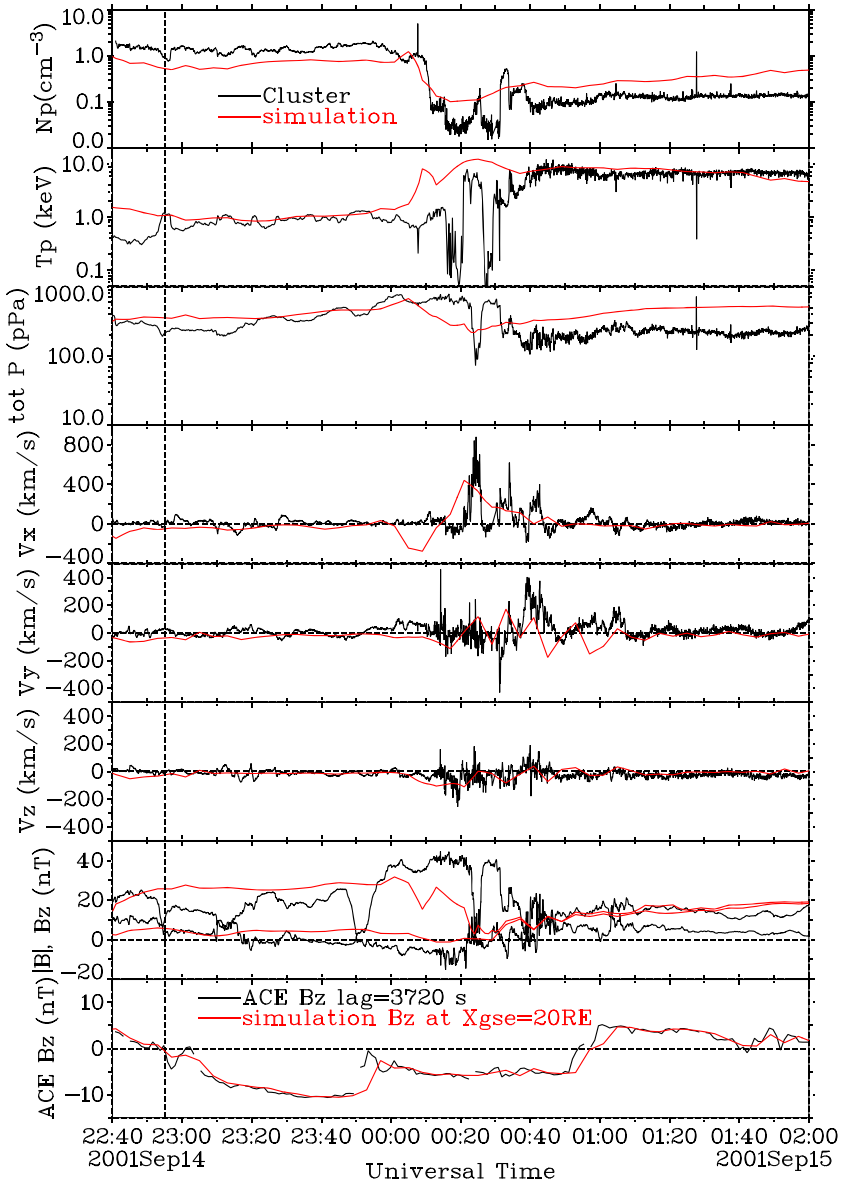

Figure 4. Cluster observations and the corresponding simulation results from 22:40:00 UT on 14 September to 02:00:00 UT on 15 September 2001. Shown from top to bottom are plasma density, plasma temperature, plasma pressure + magnetic pressure, plasma velocity *x*, *y*, and *z* components, magnetic field magnitude, and *z* component, and the shifted IMF B_z at ACE. All values are in GSE coordinates. The simulation results have been shifted 25 min forward.

flow velocity. The dipolization of the tail field at geosynchronous orbit was observed at 00:15 UT, after which the plasma density gradually decreased. The period during which the magnetic field stretched and built up at all three geosynchronous spacecraft is almost the same as the period during which Cluster observed the stretched magnetic field. During this period, the convection of the previously stagnant plasma flow was significantly enhanced at all LANL satellites and Cluster locations.

3.5. Related Auroral Observations

The NASA IMAGE spacecraft observed an auroral substorm event commencing at 23:52:24 UT on 14 September 2001. During the 23 h before ~23:00:00 UT, the polar cap was calm and no auroral disturbances were observed (the auroral images are not shown here), as a result of the long period of northward IMF during this day. After ~23:00:00 UT, by which the southward IMF had arrived at the magnetopause, the auroral oval started to grow slightly. At 00:10:49 UT the next day, the auroral oval suddenly brightened in comparison with

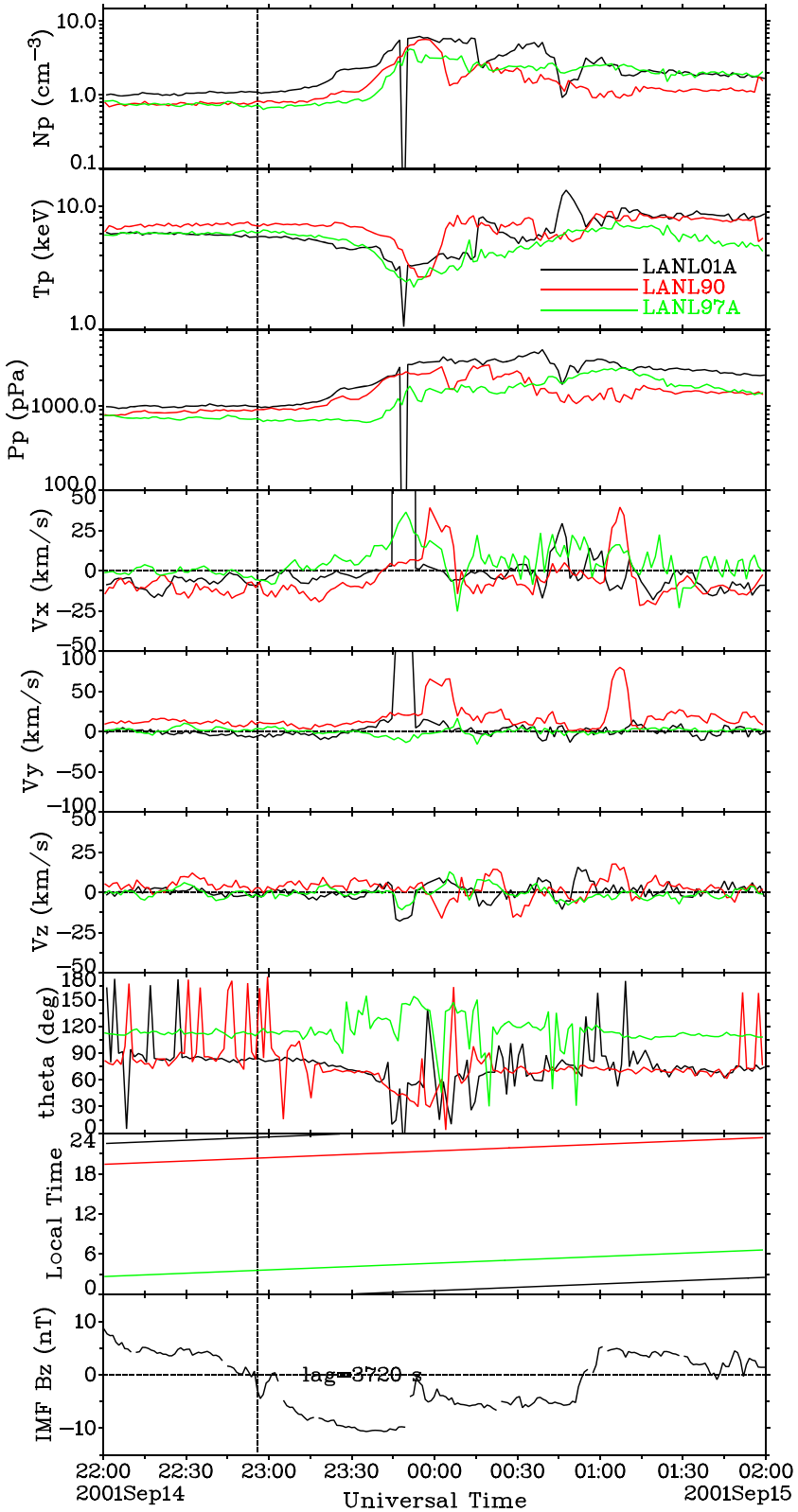

Figure 5. The observations of LANL spacecraft from 22:00:00 UT on 14 September 2001 to 02:00:00 UT on 15 September 2001. Shown from top to bottom are plasma density; plasma temperature; plasma pressure; plasma velocity GSE *x*, *y*, and *z* components; the angle from the radial direction toward the Earth to the magnetic field direction; the local time position; and the shifted ACE magnetic field GSE *z* component.

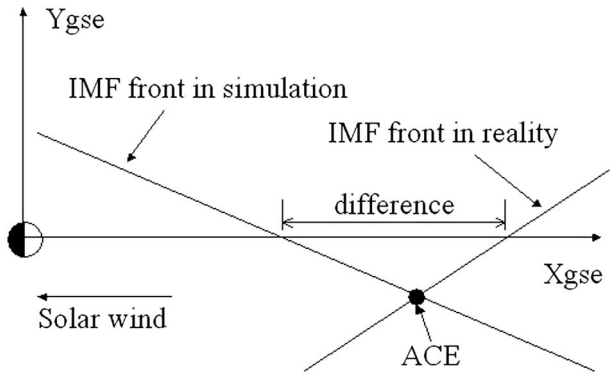

Figure 6. A possible IMF front in simulation or in reality. An IMF front in the simulation may arrive at the magnetopause earlier than the actual arrival time for an amount of time related to the spatial difference indicated in the figure and the corresponding solar wind speed.

the previous image at 23:56:29 UT. The dawnside aurora was substantially enhanced. That means a substorm onset occurred. Note that the CDPS at Cluster disappeared at ~00:10:00 UT. The auroral images show that the auroral substorm lasted until ~02:00:00 UT.

3.6. Ground Magnetic Disturbance

The ground magnetic disturbance related to this event is shown in the bottom panel of Figure 1. It shows the northward component of the ground magnetic field measured at some of the IMAGE magnetometer network stations. Like the auroral images, the ground measurement also shows that there was no disturbance before 23:00:00 UT that day, indicating a calm day of northward IMF condition. From 23:00:00 UT to 02:00:00 UT on the next day, the magnetometer stations were near midnight and recorded a substorm disturbance with the minimum occurring at ~00:40:00 UT.

The *Kp* index was low (<3) on 14 September as a result of the northward IMF for most of the day and then *Kp* increased after the southward turning of IMF. The *Dst* index only decreased mildly during this event.

3.7. Observation Versus Simulation

The simulation results are compared with Cluster observations in Figure 4 which shows a very high degree of agreement. The simulation reproduced the observed CDPS, the transition from a CDPS to a hot tenuous plasma sheet, and the corresponding bursty plasma flows. The simulation also captured the characteristic variation of the magnetic field which was first stretched greatly and then dipolized when a bursty flow was observed. This bursty flow was directed toward the Earth both in the observation and in the simulation.

In this simulation, the event occurred ~25 min earlier than the actual event. The main reason is that the southward IMF in the simulation arrived ~25 min earlier at the magnetopause than the actual southward IMF. The actual southward IMF arrival time at the magnetopause is 22:54 UT, as estimated in section 3.2, while the corresponding time in the simulation is ~22:29 UT. The difference in the southward IMF arrival time is caused by the different normal vectors of the IMF fronts in simulation and in actual event, as explained in Figure 6. Since there is only one solar wind monitor near the ACE orbit, it is not possible to accurately determine the IMF structure about 200 R_E ahead of the Earth. The normal vector of the IMF front was computed using minimum variance method [*Sonnerup and Cahill*, 1967, 1968].

Figures 7–9 show the comparison of simulation results with observations at geosynchronous orbit. Although there are some small discrepancies in detail, both the observations and simulation results indicate the arrival of superdense plasma (see Np and Tp panels) accompanied with small flow fluctuation (see Vx, Vy, and Vz panels) at all three LANL spacecrafts in the nightside after the southward turning of IMF. The superdense plasma arrival in the simulation is also earlier than the actual one, but the time difference is less than the difference at Cluster location. The simulated plasma density declines faster than the observed one, and the simulated temperature is higher than the actual temperature.

It is not surprising for a developing magnetosphere model to have different simulation results than observations. This version of OpenGGCM is a one-fluid MHD model without coupled inner magnetosphere model. In particular, the gradient and curvature particle drifts and the corotation electric field become significant

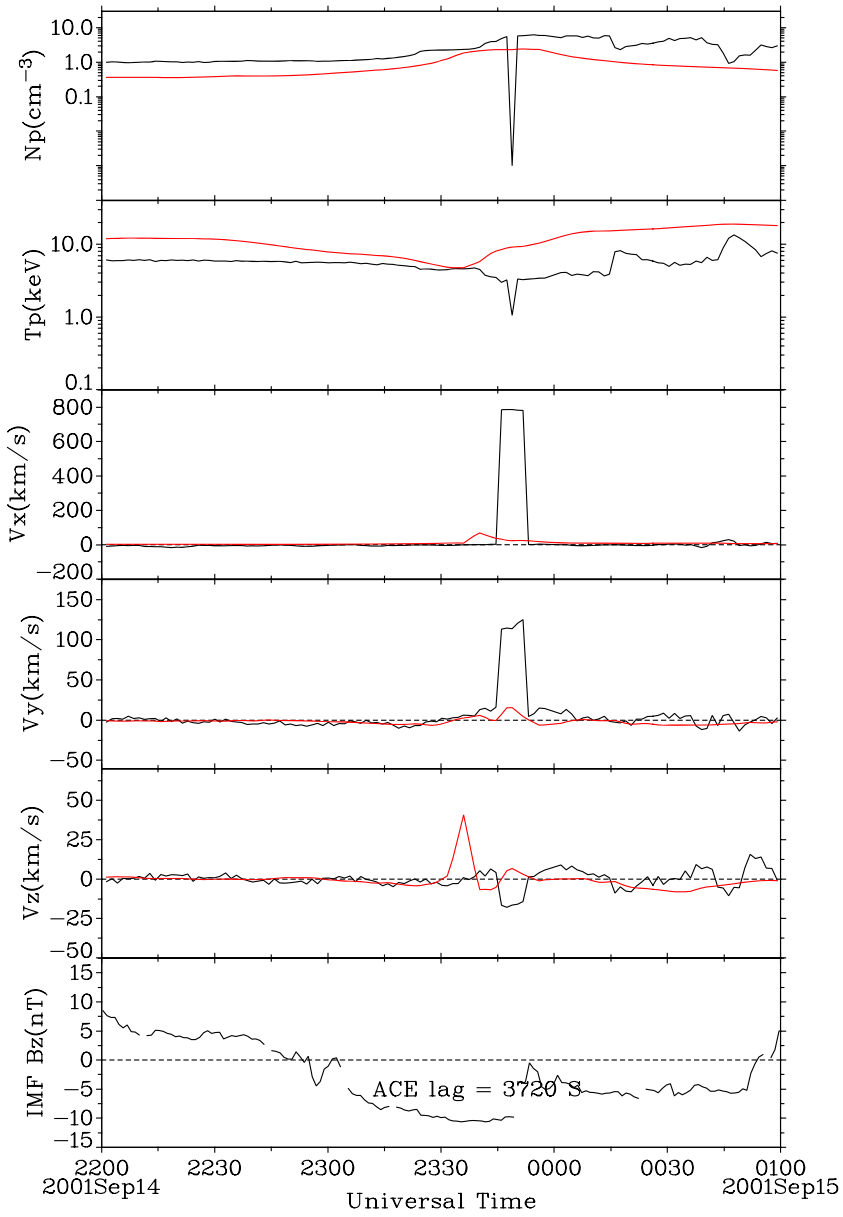

Figure 7. Simulation (red lines) versus LANL01A observations (black lines) from 22:00:00 UT on 14 September to 01:00:00 UT on 15 September. Shown from top to bottom are plasma density, temperature, three velocity components, and ACE IMF B_z with a time lag of 3720 s. The simulation results are not shifted in time here.

in the inner magnetosphere [*Korth et al.*, 1999] and are not addressed by the MHD simulation. The simulation also neglects ionospheric outflows which may become significant in the inner magnetosphere after a southward IMF arrival. During an SDPS event, there are compression and dipolization of the tail field as well as reconnection occurring near the near tail. Therefore, various waves may be generated, and wave-particle interaction, which is not included in MHD model, increases. In addition, the energetic particle fluxes at geosynchronous orbit and in the near tail, which cannot be generated in MHD model, will suddenly increase [*Quinn and Southwood*, 1982; *Mauk*, 1986; *Baker et al.*, 1984; *Moses et al.*, 1993; *Joyce et al.*, 1995; *Birn et al.*, 1997]. The reconnection rate in the simulation may be different from the real one. In section 5, we will show that the magnetic reconnection near the near tail is the key driving process to form the SDPS. The location of its diffusion region and its reconnection rate may affect the formation of the SDPS significantly. For example, if the diffusion region is closer to the Earth, less CDPS plasma material may be transported to geosynchronous orbit.

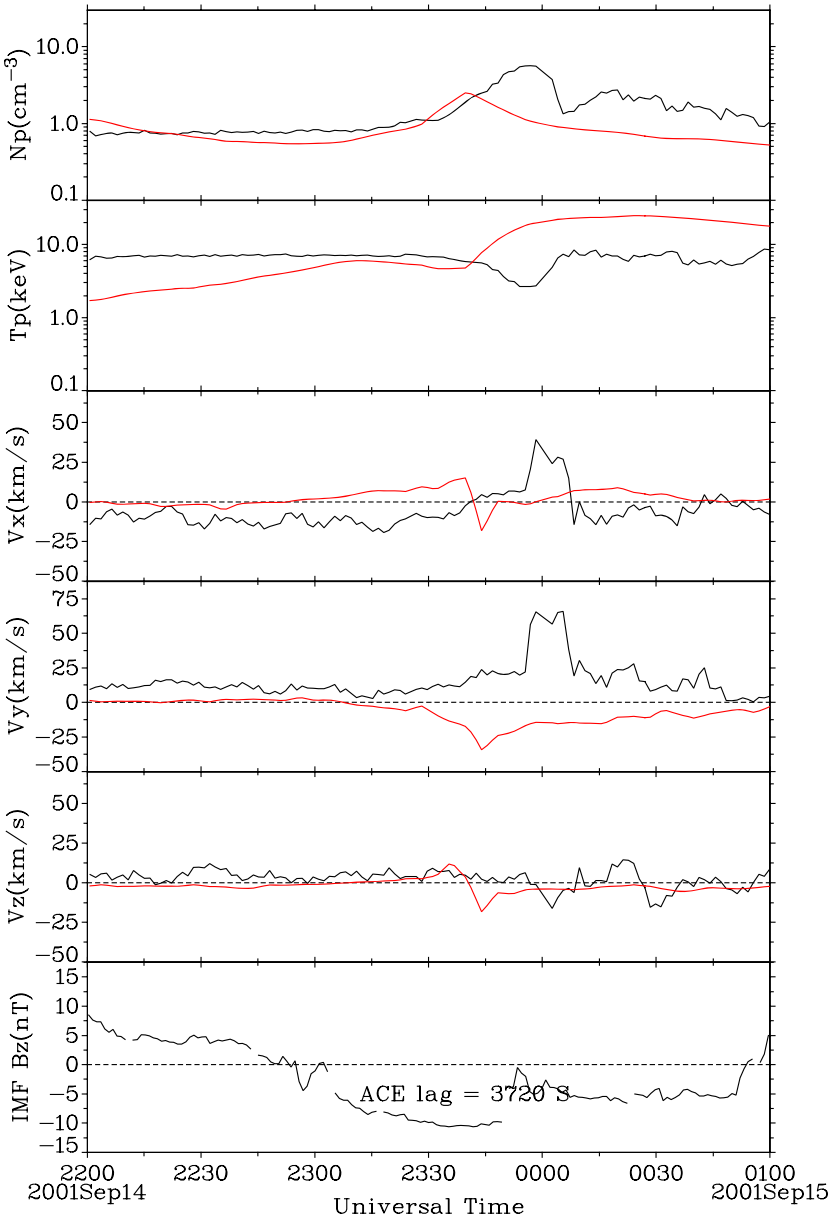

Figure 8. Simulation (red lines) versus LANL90 observations (black lines) from 22:00:00 UT on 14 September to 01:00:00 UT on 15 September. Shown are the same parameters as in Figure 7.

4. Event on 19 January 2002

This event has been discussed in detail by *Thomsen et al.* [2003]. Here we only give a brief introduction. At ~10:30 UT the IMF turned southward at ACE, simultaneous with a sudden density enhancement. Before this time, the IMF *z* component was northward from the beginning of the day. LANL-1991-080 observed an interval of cool (~3 keV), superdense (~4 cm^{-3}) plasma sheet from ~12:30 UT to ~13:30 UT in the near-midnight region of geosynchronous orbit. The cool, superdense plasma sheet was subsequently encountered near dusk by satellites LANL-1994-084 and LANL-02A. The NASA IMAGE spacecraft observed a substorm at 12:45:55 UT.

An OpenGGCM simulation was run for this event with the same setting as the simulation of the event on 14 September 2001. Both the observations and simulation results shown in Figure 10 show that a superdense plasma sheet appeared at the location of LANL-1991-080 in the near-midnight region of the geosynchronous orbit. This simulation further confirms that OpenGGCM can reproduce the formation of a superdense plasma sheet in the near-midnight region of geosynchronous orbit.

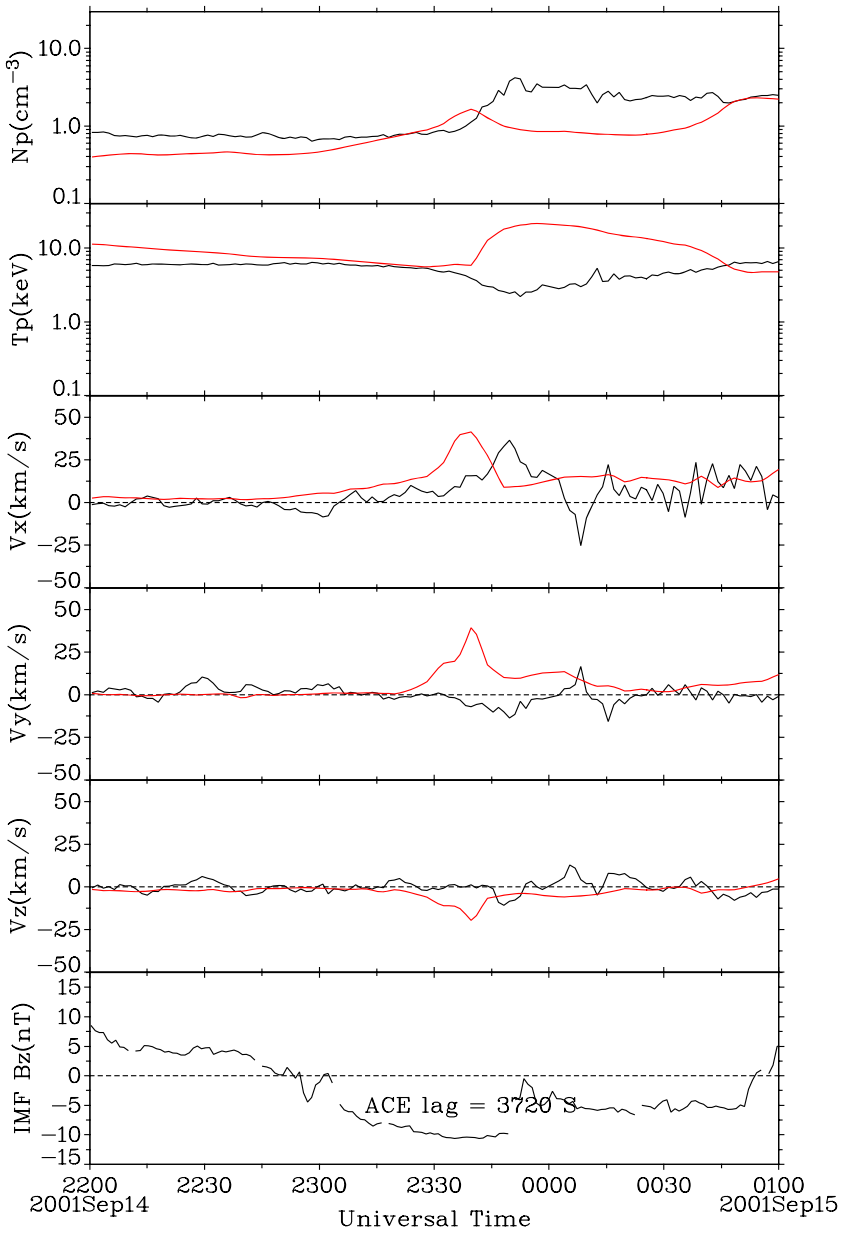

Figure 9. Simulation (red lines) versus LANL97A observations (black lines) from 22:00:00 UT on 14 September to 01:00:00 UT on 15 September. Shown are the same parameters as in Figure 7.

5. SDPS Formation Process

Both event simulations reproduced the observed superdense plasma sheet. With abundant observations from a variety of locations as well as the high-degree agreement between simulation and observations, the event on 14 September 2001 is a high-value event for studying the formation of SDPS. The comparison between the simulation results and the observations of Cluster and LANL spacecrafts indicates that this simulation reproduced the main features of SDPS event, including the formation and disappearance of a cold dense plasma sheet in the near-midnight region at ~20 R_E as well as the arrival of a superdense plasma sheet at three LANL satellites at nightside geosynchronous orbit. By analyzing these simulation results, a detailed SDPS formation process may be revealed. Figures 11–14 show plasma density and V_x on GSE equatorial plane and noon-midnight meridian at different times. They display the formation process of an SDPS. This process will be discussed in the following paragraphs in the order of time in the simulation and is referred to the corresponding frames in Figures 11–14.

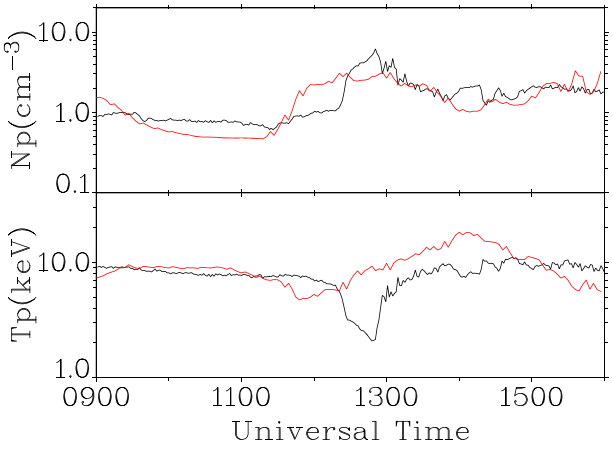

Figure 10. Simulation (red lines) versus LANL-1991-080 observations (black lines) from 09:00:00 UT to 16:00:00 UT on 19 January 2002.

At 22:28 UT in the simulation, ~2 min before the arrival of southward IMF at the magnetopause, a CDPS had been formed for an extended period of time. Figures 11a and 12a show that the plasma density of most part of the outer magnetosphere was high, at least ~1.0 cm^{-3}, after a long period of northward IMF condition. Figure 11a shows that most of the dense plasma was in a region extending from dusk flank and dawn flank of the magnetotail, in agreement with previous Geotail observations [*Fujimoto et al.*, 1998] and simulations [*Li et al.*, 2008] of CDPS events. There was also some dense plasma near the noon-midnight meridian. Such a large area of dense plasma in the midtail was in part the result of the high solar wind density which also led to high solar wind dynamic pressure and thus an unusually compressed magnetopause for such northward IMF conditions. The velocity *x* component in Figures 13a and 14a shows that the plasma flow was almost stagnant in the plasma sheet at this time. Some of the dense plasma was convecting tailward, while most of the dense plasma below ~30 R_E has a weak sunward convection. This is a typical situation when IMF is northward.

By 23:00 UT in the simulation, after ~30 min of southward IMF acting on the magnetosphere, much of the dense plasma had been depleted, especially for regions near the lobes, as indicated by Figure 12b. However, Figure 11b indicates that more dense plasma accumulated near the equatorial plane at x_{gse}=~ −20 R_E, most likely as a result of the compression of the magnetotail by dayside newly created open flux tubes convecting tailward. This compression is indicated by the enhanced total pressure and the highly stretched field during the time period from 23:20 UT to 00:20 UT in Cluster observations. At this time, the plasma convection was still weak as indicated by Figures 13b and 14b.

At 23:24 UT in the simulation, the plasma in the region indicated by a letter "b" was being depleted most likely because the dipole field was highly stretched there, and thus, the convection was strong in that region, as indicated by Figures 13c and 14c. The dense plasma in the region indicated by a letter "a" was still hanging there, but some dense plasma had come closer to midnight geosynchronous orbit to the region indicated by a letter "c."

By 23:36 UT, the reconnection due to the highly stretched dipole field had been set off in region "b" and had resulted in a hot tenuous region there, while the neighboring dense plasma was still in region "a." At this time, the corresponding Cluster position in the simulation was about GSE (−18.8, 2.88, 2.12) R_E, and was most likely in region "b." Note that, in reality, Cluster location was changing into a hot tenuous plasma region at 00:10 UT on 15 September which is corresponding to 23:36 UT on 14 September after counting in a difference of ~25 min between the simulation and the actual event. The two-dimensional magnetic field lines on the GSE XZ plane shown in Figure 15 demonstrate that the geomagnetic dipole field was being compressed, most likely resulting in a substorm onset at ~20 R_E in the tail. Figures 13d and 14d indicate that the reconnection site was most likely near region "b." At 23:36 UT in the simulation, the dense plasma arrived at geosynchronous orbit, and the sunward convection in the midnight region from Xgse ~ −20 R_E to ~ −10 R_E was much stronger than before. The dense plasma sheet began to separate into two parts from the reconnection region in Figure 14d. One part flew away toward the tail and the other part convected toward the Earth. The NASA IMAGE spacecraft observed an auroral substorm event commencing at 23:52:24 UT and a sudden

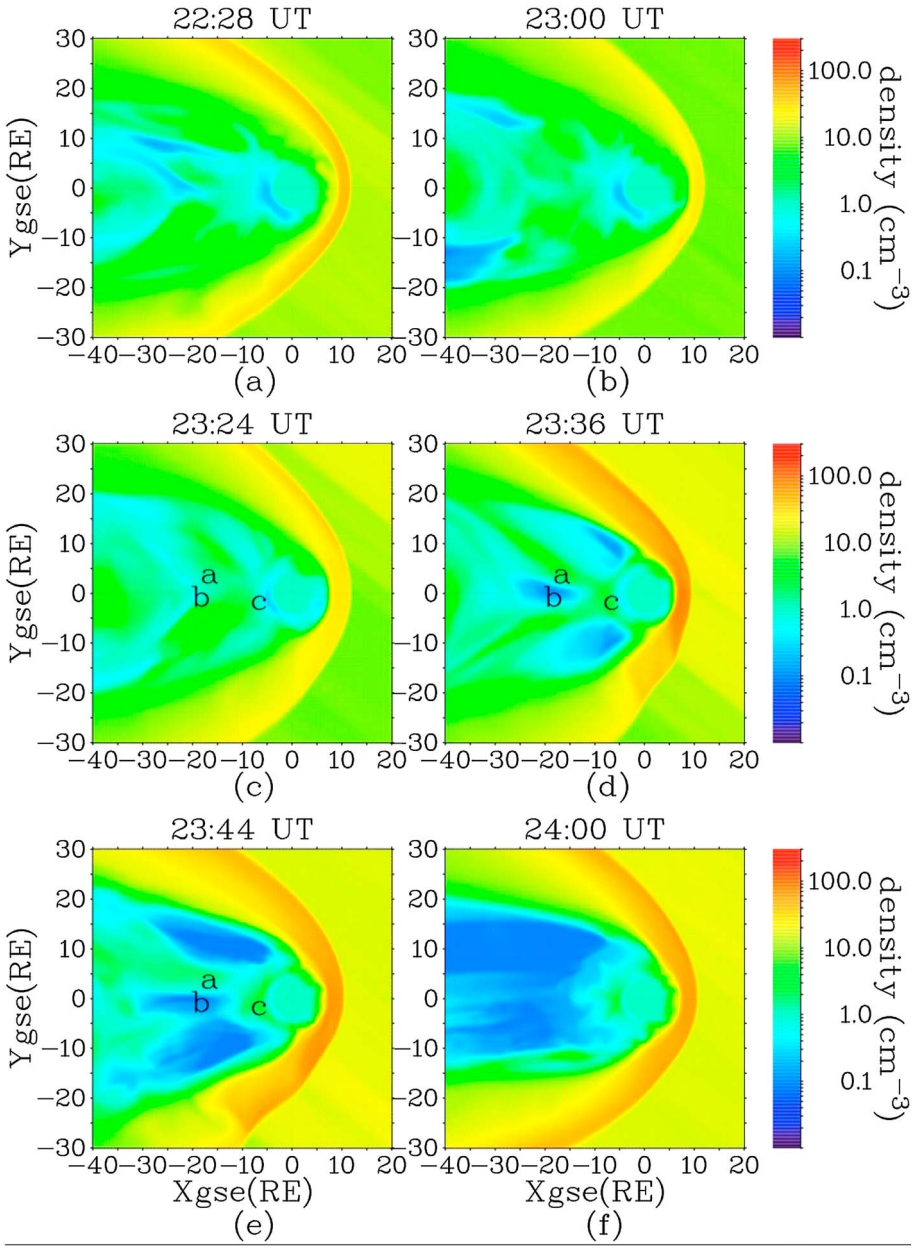

Figure 11. The simulation plasma density on GSE equatorial plane at different times during the SDPS event on 14–15 September 2001. The letters "a," "b," and "c" indicate interested areas discussed in section 5.

brightening at 00:10:49 UT. These observations agree with the simulation results shown here considering that the event occurred ~25 min earlier in the simulation than in the actual event.

At 23:44 UT, more dense plasma was approaching geosynchronous orbit in the region "c," while the dense plasma in region "a" was being depleted tailward and the hot tenuous region "b" was expanding. The plasma speed near the reconnection site was very high at this time, but the plasma there was tenuous. Therefore, there was not much dense plasma contributed to the inner magnetosphere at this time. This time roughly corresponded to the peak value of the superdense plasma at geosynchronous orbit. Around this time, bursty plasma flows began to appear.

By 24:00 UT, much of the dense plasma near geosynchronous orbit had been depleted, and most of the dense plasma in the near tail had disappeared. At this time, the near-tail reconnection process was still occurring. Without a coupled model of the inner magnetosphere, this simulation is not appropriate in describing plasma or magnetic field events within geosynchronous orbit.

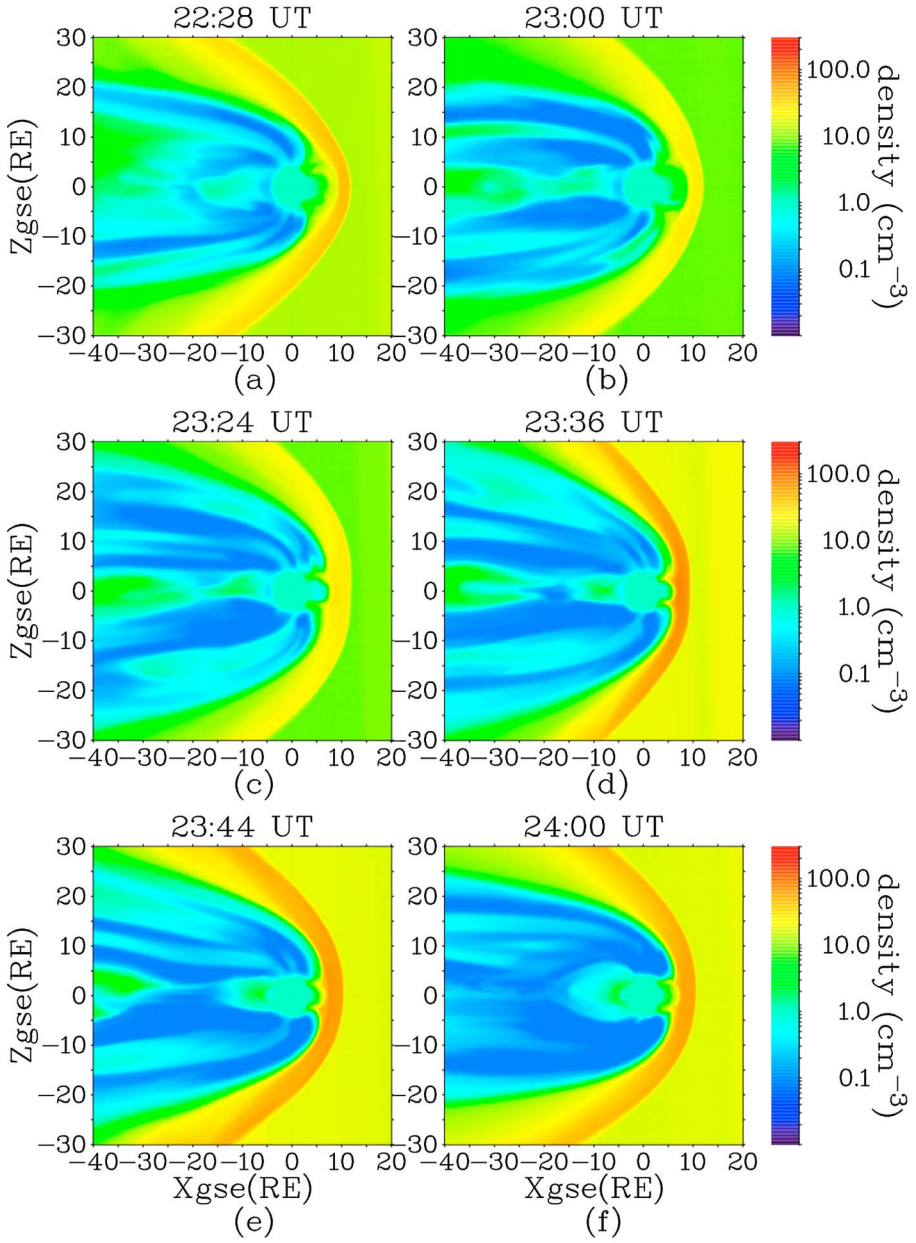

Figure 12. The simulation plasma density on noon-midnight meridian plane at different times during the SDPS event on 14–15 September 2001. The time stamps are the same as those in Figure 11.

6. Discussion

When reporting SDPS observations, *Borovsky et al.* [1997] suggested that there were three possible origins for the SDPS: ionosphere, plasmasphere, and solar wind. However, they could not determine which one was the main source. In this study, we focus on the first 3 h after the appearance of the SDPS and try to identify the main source of the SDPS in its early stage.

It is well known that ionospheric outflow is significant when *Kp* is at elevated levels [*Young et al.*, 1982; *Yau et al.*, 1985]. Elevated *Kp* is associated with southward IMF and high auroral activity. In the event of 2001, *Kp* is low (<3) before the SDPS appearance and is slightly greater than 3 after that. Therefore, ionospheric outflow should not have been particularly strong, and it is doubtful that there was enough time to accumulate plasma to achieve a density at such extreme high level (~5 cm^{-3} at midnight geosynchronous orbit). Although ionospheric outflow might provide some material in the midtail, given the low level of *Kp* before the event, ionospheric plasma is likely not dominant in the SDPS.

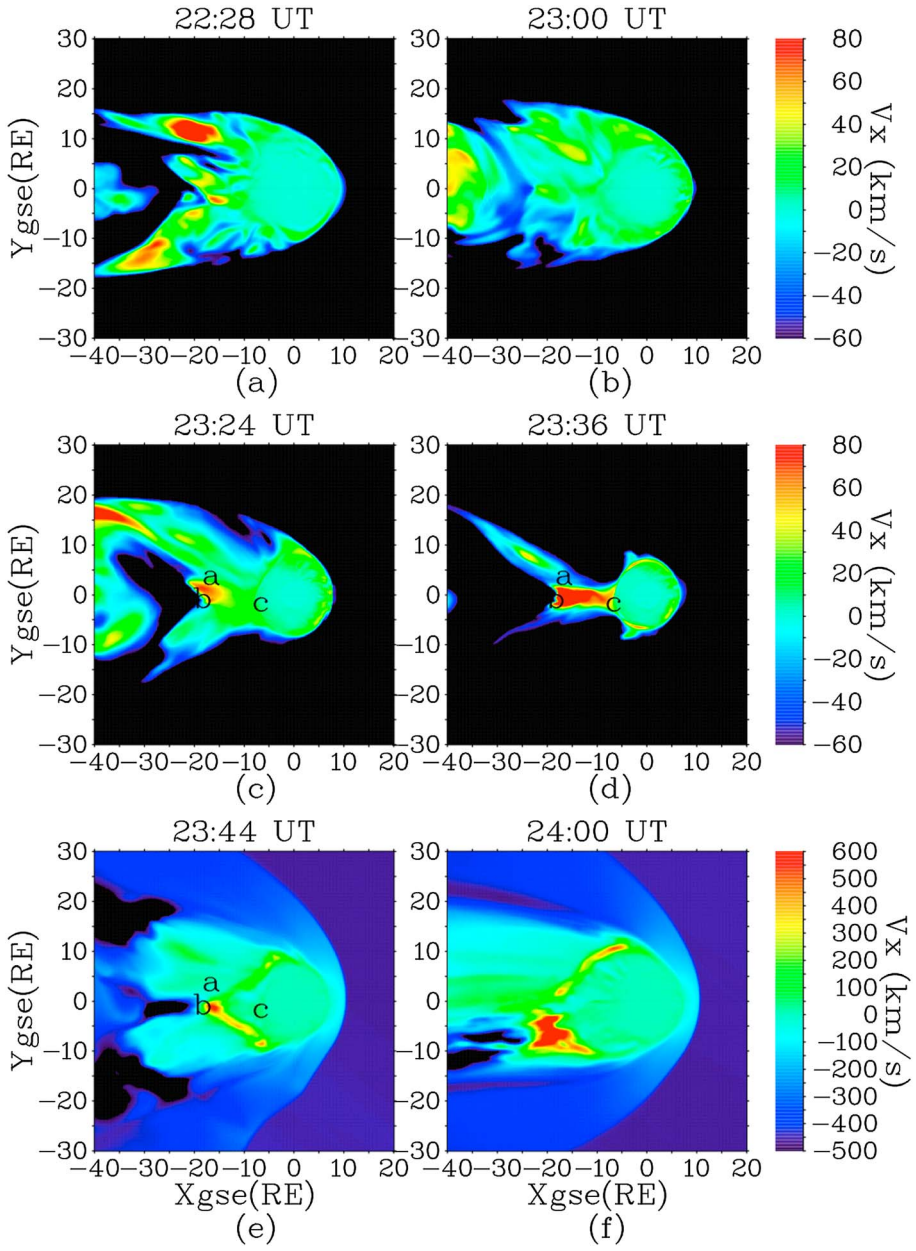

Figure 13. The simulation plasma velocity GSE *x* component on GSE equatorial plane at different times during the SDPS event on 14–15 September 2001. The time stamps and the letters are the same as those in Figure 11.

Plasmasphere refills out to large radii and thus appears at nearly all local times at geosynchronous orbit when geomagnetic activity is low for a day or two [*Sojka and Wrenn*, 1985; *Borovsky and Steinberg*, 2006]. However, the plasmasphere density at geosynchronous orbit is usually greater than 10 cm^{-3} and lasts for many hours. Since the plasma density of SDPS in the presented events was less than 10 cm^{-3} and the superdense plasma appeared after the arrival of southward IMF, the superdense plasma was not a direct result of a plasmasphere refill, although the magnetosphere had been quiet under northward IMF conditions for at least 1 day before the SDPS appearance. *Borovsky et al.* [1997] suggested a multistep path whereby plasma goes from plasmasphere to the dayside and then to the nightside through open flux tubes as a result of dayside reconnection when IMF is southward. Such a path would take at least several hours. It is not able to transport sufficient plasma from the plasmasphere to form a plasma sheet with extremely high level of ~5 cm^{-3} within 1 h of the arrival of the southward IMF.

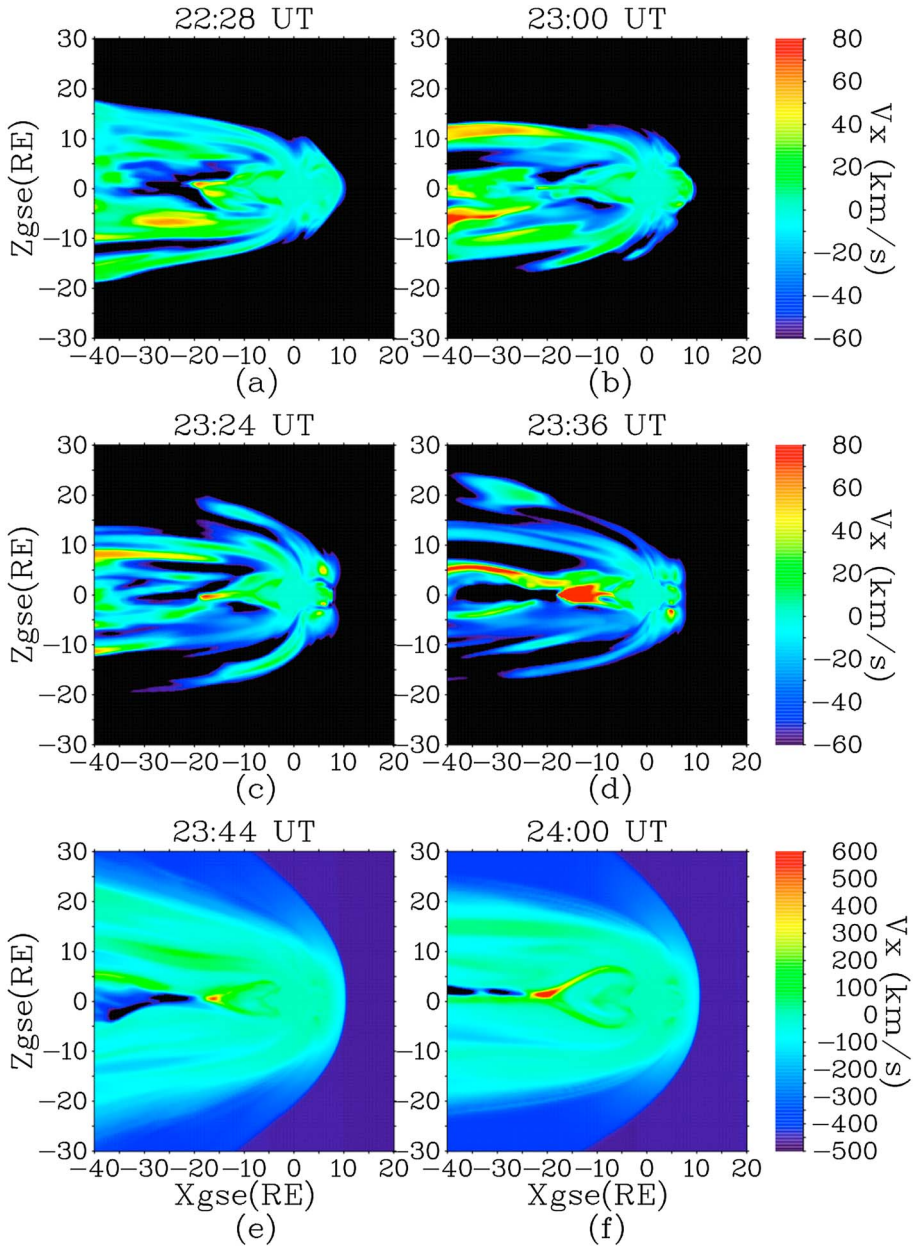

Figure 14. The simulation plasma velocity GSE *x* component on GSE noon-midnight meridian plane at different times during the SDPS event on 14–15 September 2001. The time stamps are the same as those in Figure 11.

The high level of solar wind density before and after the appearance of SDPS indicates that solar wind is possibly the dominant origin. There are two scenarios for solar wind plasma entry into geosynchronous orbit. One scenario is that the very dense solar wind plasma coming with the southward IMF contributes directly to SDPS. The other scenario is that solar wind plasma enters into the midtail when the IMF is northward and then is compressed and convected sunward after the IMF turns southward. The following two paragraphs will discuss which scenario has the dominant effect on the formation of SDPS in the studied events.

It usually takes about 1 h for a footprint of an open flux tube created from dayside magnetopause reconnection to move from the dayside to the nightside across the polar cap since the Dungey convection cycle takes about 3 h [*Q.-H. Zhang et al.*, 2015]. Therefore, the very dense plasma from the magnetosheath is not likely able to form an extremely dense plasma sheet in the nightside of geosynchronous orbit within 1 h. Note that from the time of southward IMF turning to the time of appearance of plasma sheet with a density of 2 cm^{-3} there is only ~30 min as shown in Figure 1. The solar wind speed was about 500 km/s, which is moderate. The plasma

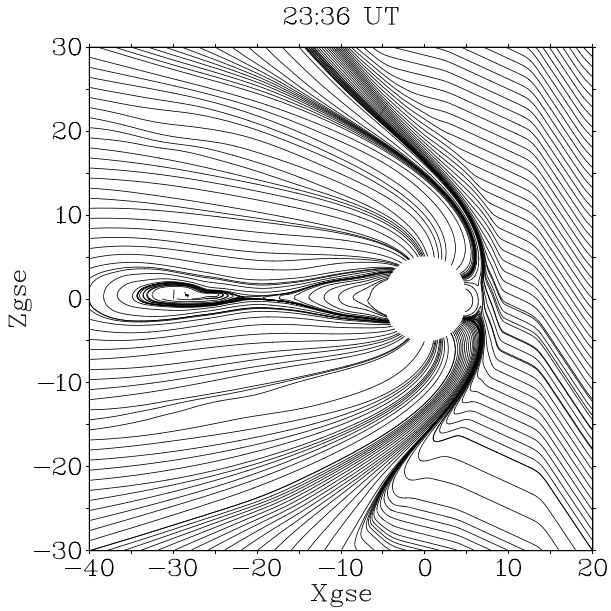

Figure 15. The simulation 2-D magnetic field lines on GSE noon-midnight meridian plane at 23:36:00 UT for the event on 14–15 September 2001.

density distribution in Figures 11c–11e or Figures 12c–12e shows that the dense solar wind plasma does not have significant effect on the magnetotail lobes and the plasma sheet. The magnetosheath density may be extremely high (100–125 cm^{-3}) when the solar wind density is very high as shown in Figures 11 and 12. However, these two figures also show that the extremely high density in the magnetosheath does not significantly affect the density in the mantle and low-latitude boundary layer. Instead, the boundary is sharper (density gradient in normal direction is larger) when IMF turns southward. The very low density lobe regions between the magnetopause and the plasma sheet expanded after the arrival of southward IMF. These lobe regions also indicate that massive and efficient plasma entry through diffusion across the magnetopause does not likely occur. The very dense solar wind plasma coming with the southward IMF is thus unlikely to contribute directly to the SDPS within the first 3 h.

One significant fact regarding the two presented events is that IMF was northward for a long period before the appearance of the SDPS. It is well known that a cold (<1 keV) dense (~1 cm^{-3}) plasma sheet (CDPS) forms near the midtail under northward IMF conditions. Such cold dense plasma material may appear at the center of the midtail when the solar wind density level is high, as shown in Figure 11a. The CDPS constitutes a main source for SDPS. Since such cold dense plasma material forms in the near midtail after an extensive period of northward IMF, especially with very dense solar wind plasma, a moderate compression and convection may efficiently transport this material to geosynchronous orbit and form an SDPS in the more inner magnetosphere, as shown in section 5. This scenario is strongly supported by a list of SDPS events reported by *Thomsen et al.* [2003] that have at least 3 h of northward IMF followed by a southward turning. *Borovsky and Steinberg* [2006] showed that cold dense material could be seen at geosynchronous orbit after convection commences in the early phase of recurring high-speed-stream-driven storms during which SDPS events are common and before which a calm (low *Kp*) period is also common. *Lavraud et al.* [2005] reported events during which cold dense (>2 cm^{-3}) plasma material was observed at geosynchronous orbit for approximately 1–2 h after the appearance of SDPS. All these studies strongly indicate that cold dense plasma entering the midtail region during northward IMF conditions is the main direct source of SDPS in its early stage after an IMF southward turning. One should note that most of the CDPS plasma material is transported tailward in the simulations. *Lavraud et al.* [2005] showed that CDPS dense plasma accessing to geosynchronous orbit does not necessarily result in a stronger ring current for generally low convection enhancements, but *Lavraud et al.* [2006b] showed that the ring current is larger if CDPS and SDPS are present during actual storm times.

It is known that there are two important mechanisms that may lead to the formation of a CDPS: (1) diffusive process (Kelvin-Helmholtz) along the tail flank [*Terasawa et al.*, 1997; *Fairfield et al.*, 2000; *Fujimoto and Terasawa*, 1994; *Nykyri and Otto*, 2001; *Nykyri et al.*, 2006; *Hasegawa et al.*, 2004; *Kavosi and Raeder*, 2015] and (2) entry

through high-latitude reconnection between the lobe field and the northward IMF at both hemispheres [*Song and Russell*, 1992; *Song et al.*, 1999; *Raeder et al.*, 1995, 1997; *Onsager et al.*, 2001; *Li et al.*, 2005; *Lavraud et al.*, 2006c]. Substorm, the main process of solar wind entry during southward IMF condition, was not supposed to occur during northward IMF condition. However, recent observations have shown that substorms did occur during northward IMF condition [*Du et al.*, 2008; *Lee et al.*, 2010; *Park et al.*, 2010; *Peng et al.*, 2013; *L. Q. Zhang et al.*, 2015; *Park et al.*, 2015]. Such substorms may significantly facilitate solar wind entry in the magnetotail during northward IMF condition. In this study, the CDPS formed in the simulations mainly due to mechanism (2) because the simulation settings are not sufficient to generate Kelvin-Helmholtz waves. However, the simulation of event 2001 creates a CDPS that agrees well with Cluster observations as show in Figure 4. Also, using OpenGGCM simulation, *Li et al.* [2005] earlier showed that mechanism (2) can form a CDPS that agrees well with Cluster observations. It is possible that mechanism (1) may contribute some solar wind plasma to the CDPS. However, how CDPS forms does not affect our conclusion here. While this scenario was proposed previously based on observations, we here use combined observations and simulations to show that if a CDPS has formed in the midtail, it can indeed be transported deeper in the magnetosphere through geosynchronous orbit if sufficient convection is set up by the southward turning of the IMF.

7. Summary

We have studied the formation mechanism of a superdense plasma sheet detected at geosynchronous orbit in association with the IMF turning southward after a long period of northward direction. Using OpenGGCM MHD model, we simulated two SDPS events occurred on 14–15 September 2001 and on 19 January 2002. The observation data sets for the first event are from ACE, Wind, Cluster, LANL geosynchronous spacecraft, NASA IMAGE, and ground magnetometer stations. These observations show a chain of events in regions from the near tail to the ground in responding to the arrival of southward IMF following a long period of northward IMF condition. The simulation results for the first event agree well with the observations. Therefore, the simulation results in combination with observations allow us to discuss in detail the formation process of an SDPS. The simulation of the second event gives us confirmation that OpenGGCM is able to simulate an SDPS event with similar IMF conditions. Although not shown here, the plasma density, velocity, and magnetic field profiles of this event also display similar process during which cold dense plasma sheet, near-tail reconnection, and superdense plasma sheet all occur consequently.

Here we try to describe the formation of an SDPS for its early stage. An extended period of northward IMF causes solar wind plasma to enter the magnetosphere as a result of double high-latitude reconnection and probably Kelvin-Helmholtz instability along the magnetotail flanks. The relatively cold and dense plasma entering from the magnetosheath comes near to the tail flanks and in the near-tail plasma sheet, and some intrudes into a region near midnight local time. A subsequent southward IMF first causes newly created open flux tubes convecting tailward from dayside magnetopause to compress the plasma sheet and enhance its plasma convection. Some of the existing dense plasma near midnight is thus compressed toward the equatorial plane and convected toward the Earth at the same time by the enhanced electric field. The continuing compression of the lobes and the plasma sheet then causes the onset of a reconnection in the near-tail plasma sheet. The enhanced convection caused by the reconnection then pushes more dense plasma toward the Earth and causes the formation of a superdense plasma sheet near nightside geosynchronous orbit. Approximately after the cold dense plasma material near the near tail is depleted by the reconnection, the SDPS reaches its density peak value within ~3 h after its appearance and then begins to decay. The major source of the presented SDPS is from previously formed CDPS under northward IMF condition rather than directly from superdense solar wind under southward IMF condition.

Acknowledgments
The authors would like to thank the ACE team, the Wind team, NASA Imager for Magnetopause-to-Aurora Global Exploration, and International Monitor for Aurora Geomagnetic Effects for providing their data. Computations were performed on the Zaphod Beowulf cluster which was in part funded by the Major Research Instrumentation program of the National Science Foundation under grant ATM-0420905. The work by Wen-Hui Li, Lian-Zhong Lü, and En-Wei Liang has been supported by the Chinese Guangxi Science Foundation (2013GXNSFFA019001). The work by Wen-Hui Li was also supported by LANL IGPP mini-grant 1518 and by NSF GEM grant ATM 0503189. The data used are available from the corresponding author on request.

References

Angelopoulos, V., W. Baumjohann, C. F. Kennel, F. V. Coroniti, M. G. Kivelson, R. Pellat, R. J. Walker, H. Lühr, and G. Paschmann (1992), Bursty bulk flows in the inner central plasma sheet, *J. Geophys. Res.*, *97*, 4027–4039, doi:10.1029/91JA02701.

Baker, D. N., S.-I. Akasofu, W. Baumjohann, J. W. Bieber, D. H. Fairfield, E. W. Hones, B. H. Mauk, R. L. McPherron, and T. Moore (1984), Substorms in the magnetosphere, in *Solar Terrestrial Physics – Present and Future*, edited by D. M. Butler and K. Papadopoulos, pp. 8-1–8-55, chap. 8., NASA Ref. Publ., NASA RP-1120, Washington, D. C.

Baumjohann, W., G. Paschmann, and C. A. Cattell (1989), Average plasma properties in the central plasma sheet, *J. Geophys. Res.*, *94*, 6597–6606.

Birn, J., M. Thomsen, J. Borovsky, G. Reeves, D. McComas, R. Belian, and M. Hesse (1997), Substorm ion injections: Geosynchronous observations and test particle orbits in three-dimensional dynamic MHD fields, *J. Geophys. Res.*, *102*, 2325–2341, doi:10.1029/96JA03032.

Borovsky, J. E., and J. T. Steinberg (2006), The "calm before the storm" in CIR/magnetosphere interactions occurrence statistics, solar wind statistics, and magnetospheric preconditioning, *J. Geophys. Res.*, *111*, A07S10, doi:10.1029/2005JA011.397.
Borovsky, J. E., M. F. Thomsen, and D. J. McComas (1997), The superdense plasma sheet: Plasmaspheric origin, solar wind origin, or ionospheric origin?, *J. Geophys. Res.*, *102*, 22,089–22,097, doi:10.1029/96JA02469.
Borovsky, J. E., M. F. Thomsen, D. J. McComas, T. E. Cayton, and D. J. Knipp (1998a), Magnetospheric dynamics and mass flow during the November 1993 storm, *J. Geophys. Res.*, *103*, 26,373–26,394, doi:10.1029/97JA03051.
Borovsky, J. E., M. F. Thomsen, R. C. Elphic, T. E. Cayton, and D. J. McComas (1998b), The transport of plasma sheet material from the distant tail to geosynchronous orbit, *J. Geophys. Res.*, *103*, 20,297–20,331, doi:10.1029/97JA03144.
Denton, M. H., J. E. Borovsky, R. M. Skoug, M. F. Thomsen, B. Lavraud, M. G. Henderson, R. L. McPherron, J. C. Zhang, and M. W. Liemohn (2006), Geomagnetic storms driven by ICME- and CIR-dominated solar wind, *J. Geophys. Res.*, *111*, A07S07, doi:10.1029/2005JA011.436.
Du, A. M., B. T. Tsurutani, and W. Sun (2008), Anomalous geomagnetic storm of 21–22 January 2005: A storm main phase during northward IMFs, *J. Geophys. Res.*, *113*, A10214, doi:10.1029/2008JA013.284.
Ebihara, Y., M.-C. Fok, R. A. Wolf, M. F. Thomsen, and T. E. Moore (2005), Nonlinear impact of plasma sheet density on the storm-time ring current, *J. Geophys. Res.*, *110*, A02208, doi:10.1029/2004JA010.435.
Fairfield, D. H., R. P. Lepping, E. W. Hones, S. J. Bame, and J. R. Asbridge (1981), Simultaneous measurements of magnetotail dynamics by IMP spacecraft, *J. Geophys. Res.*, *86*, 1396–1414, doi:10.1029/JA086iA03p01396.
Fairfield, D. H., A. Otto, T. Mukai, S. Kokubun, R. P. Lepping, J. T. Steinberg, A. J. Lazarus, and T. Yamamoto (2000), Geotail observations of the Kelvin-Helmholtz instability at the equatorial magnetotail boundary for parallel northward fields, *J. Geophys. Res.*, *105*, 21,159–21,173, doi:10.1029/1999JA000316.
Fujimoto, M., and T. Terasawa (1994), Anomalous ion mixing within an MHD scale Kelvin-Helmholtz vortex, *J. Geophys. Res.*, *99*, 8601–8613, doi:10.1029/93JA02722.
Fujimoto, M., A. Nishida, T. Mukai, Y. Saito, T. Yamamoto, and S. Kokubun (1996), Plasma entry from the flanks of the near-Earth magnetotail: Geotail observations in the dawnside LLBL and the plasma sheet, *J. Geomagn. Geoelectr.*, *48*, 711–727.
Fujimoto, M., T. Terasawa, T. Mukai, Y. Saito, T. Yamamoto, and S. Kokubun (1998), Plasma entry from the flanks of the near-Earth magnetotail: Geotail observations, *J. Geophys. Res.*, *103*, 4391–4408, doi:10.1029/97JA03340.
Fujimoto, M., T. Mukai, and S. Kokubun (2002), The structure of the plasma sheet under northward IMF, in *Frontiers in Magnetospheric Plasma Physics*, edited by M. Hoshino, Y. Omura, and L. J. Lanzerotti, pp. 19–27, COSPAR, Kanagawa, Japan.
Fuller-Rowell, T. J., D. Rees, S. Quegan, R. J. Moffett, M. V. Codrescu, and G. H. Millward (1996), A coupled thermosphere-ionosphere model (CTIM), in *STEP Report*, edited by R. W. Schunk, pp. 217, Scientific Committee on Solar Terrestrial Physics (SCOSTEP), NOAA/NGDC, Boulder, Colo.
Fuselier, S. A., R. C. Elphic, and J. T. Gosling (1999), Composition measurements in the dusk flank magnetosphere, *J. Geophys. Res.*, *104*, 4515–4522, doi:10.1029/1998JA900.137.
Hasegawa, H., M. Fujimoto, T. D. Phan, H. Rème, A. Balogh, M. W. Dunlop, C. Hashimoto, and R. TanDokoro (2004), Transport of solar wind into Earth's magnetosphere through rolled-up Kelvin-Helmholtz vortices, *Nat. Commun.*, *430*, 755–758.
Jordanova, V. K., C. J. Farrugia, L. Janoo, J. M. Quinn, R. B. Torbert, K. W. Olgilvie, R. P. Lepping, J. T. Steinberg, D. J. McComas, and R. D. Belian (1998), October 1995 magnetic cloud and accompanying storm activity: Ring current evolution, *J. Geophys. Res.*, *103*, 79–92, doi:10.1029/97JA02367.
Joyce, G., J. Chen, S. Slinker, D. Holland, and J. Harold (1995), Particle energization near an X line in the magnetotail based on global MHD fields, *J. Geophys. Res.*, *100*, 19,167–19,176, doi:10.1029/95JA00963.
Kavosi, S., and J. Raeder (2015), Ubiquity of Kelvin-Helmholtz waves at Earth's magnetopause, *Nat. Commun.*, *6*, 7019, doi:10.1038/ncomms8019.
Korth, H., M. F. Thomsen, J. E. Borovsky, and D. J. McComas (1999), Plasma sheet access to geosynchronous orbit, *J. Geophys. Res.*, *104*, 25,047–25,061.
Kozyra, J. U., V. Jordanova, J. Borovsky, M. Thomsen, D. Knipp, D. Evans, D. McComas, and T. Cayton (1998), Effects of a high-density plasma sheet on ring current development during the November 2–6, 1993, magnetic storm, *J. Geophys. Res.*, *103*, 26285–26305.
Lavraud, B., and V. K. Jordanova (2007), Modeling the effects of cold-dense and hot-tenuous plasma sheet on proton ring current energy and peak location, *Geophys. Res. Lett.*, *34*, L02102, doi:10.1029/2006GL027.566.
Lavraud, B., M. H. Denton, M. F. Thomsen, J. E. Borovsky, and R. H. W. Friedel (2005), Superposed epoch analysis of dense plasma access to geosynchronous orbit, *Ann. Geophys.*, *23*, 2519–2529.
Lavraud, B., M. F. Thomsen, S. Wing, M. Fujimoto, M. H. Denton, J. E. Borovsky, A. Aasnes, K. Seki, and J. M. Weygand (2006a), Observation of two distinct cold, dense ion populations at geosynchronous orbit: Local time asymmetry, solar wind dependence and origin, *Ann. Geophys.*, *24*, 3451–3465.
Lavraud, B., M. F. Thomsen, J. E. Borovsky, M. H. Denton, and T. I. Pulkkinen (2006b), Magnetosphere preconditioning under northward IMF: Evidence from the study of coronal mass ejection and corotating interaction region geoeffectiveness, *J. Geophys. Res.*, *111*, A09208, doi:10.1029/2005JA011.566.
Lavraud, B., M. F. Thomsen, B. Lefebvre, S. J. Schwartz, K. Seki, T. D. Phan, Y. L. Wang, A. Fazakerley, H. Rème, and A. Balogh (2006c), Evidence for newly closed magnetosheath field lines at the dayside magnetopause under northward IMF, *J. Geophys. Res.*, *111*, A05211, doi:10.1029/2005JA011.266.
Lee, D.-Y., K.-C. Choi, S. Ohtani, J. H. Lee, K. C. Kim, K. S. Park, and K.-H. Kim (2010), Can intense substorms occur under northward IMF conditions?, *J. Geophys. Res.*, *115*, A01211, doi:10.1029/2009JA014.480.
Lennartsson, W. (1992), A scenario for solar wind penetration of Earth's magnetic tail based on ion composition data from the ISEE 1 spacecraft, *J. Geophys. Res.*, *97*, 19,221–19,238.
Li, W., J. Raeder, J. Dorelli, M. Øieroset, and T. D. Phan (2005), Plasma sheet formation during long period of northward IMF, *Geophys. Res. Lett.*, *32*, L12S08, doi:10.1029/2004GL021.524.
Li, W., J. Raeder, M. F. Thomsen, and B. Lavraud (2008), Solar wind plasma entry into the magnetosphere under northward IMF conditions, *J. Geophys. Res.*, *113*, A04204, doi:10.1029/2007JA012.604.
Li, W., J. Raeder, M. Øieroset, and T. D. Phan (2009), Cold dense magnetopause boundary layer under northward IMF: Results from THEMIS and MHD simulations, *J. Geophys. Res.*, *114*, A00C15, doi:10.1029/2008JA013.497.
Liemohn, M. W., J.-C. Zhang, M. F. Thomsen, J. E. Borovsky, J. U. Kozyra, and R. Ilie (2008), Plasma properties of superstorms at geosynchronous orbit: How different are they?, *Geophys. Res. Lett.*, *35*, L06S06, doi:10.1029/2007GL031.717.
Mauk, B. H. (1986), Quantitative modeling of the "convection surge" mechanism of ion acceleration, *J. Geophys. Res.*, *91*, 13,423–13,431.
Moses, R. W., J. M. Finn, and K. M. Ling (1993), Plasma heating by collisionless magnetic reconnection: Analysis and computation, *J. Geophys. Res.*, *98*, 4013–4040.

Nykyri, K., and A. Otto (2001), Plasma transport at the magnetospheric boundary due to reconnection in Kelvin-Helmholtz vortices, *Geophys. Res. Lett.*, *28*, 3565–3568, doi:10.1029/2001GL013239.
Nykyri, K., A. Otto, B. Lavraud, C. Mouikis, L. M. Kistler, A. Balogh, and H. Rème (2006), Cluster observations of reconnection due to the Kelvin-Helmholtz instability at the dawnside magnetospheric flank, *Ann. Geophys.*, *24*(10), 2619–2643.
Øieroset, M., T. D. Phan, M. Fujimoto, L. Chan, R. P. Lin, and R. Skoug (2002), Spatial and temporal variations of the cold dense plasma sheet: Evidence for a low-latitude boundary layer source?, in *AGU Monograph on Earth's Low-Latitude Boundary Layer*, vol. 133, edited by P. T. Newell and T. G. Onsager, pp. 253, AGU, Washington, D. C., doi:10.1029/133GM25.
Øieroset, M., J. Raeder, T. D. Phan, S. Wing, J. P. McFadden, W. Li, M. Fujimoto, H. Rème, and A. Balogh (2005), Global cooling and densification of the plasma sheet during an extended period of purely northward IMF on October 22–24, 2003, *Geophys. Res. Lett.*, *32*, L12S07, doi:10.1029/2004GL021523.
Øieroset, M., T. D. Phan, V. Angelopoulos, J. P. Eastwood, J. P. McFadden, D. Larson, C. W. Carlson, K. H. Glassmeier, M. Fujimoto, and J. Raeder (2008), THEMIS multi-spacecraft observations of magnetosheath plasma penetration deep into the dayside low-latitude magnetosphere for northward and strong By IMF, *Geophys. Res. Lett.*, *35*, L17S11, doi:10.1029/2008GL033.661.
Onsager, T. G., J. D. Scudder, M. Lockwood, and C. T. Russell (2001), Reconnection at the high-latitude magnetopause during northward interplanetary magnetic field conditions, *J. Geophys. Res.*, *106*, 25,467–25,488.
Park, K. S., T. Ogino, and Y. H. Kim (2010), Effect of the dipole tilt and northward and duskward IMF on dayside magnetic reconnection in a global MHD simulation, *J. Geophys. Res.*, *115*, A02208, doi:10.1029/2009JA014.212.
Park, K. S., D.-Y. Lee, T. Ogino, and D. H. Lee (2015), MHD simulations using average solar wind conditions for substorms observed under northward IMF conditions, *J. Geophys. Res. Space Physics*, *120*, 7672–7686, doi:10.1002/2015JA021.005.
Peng, Z., C. Wang, Y. F. Yang, H. Li, Y. Q. Hu, and J. Du (2013), Substorms under northward interplanetary magnetic field: Statistical study, *J. Geophys. Res.*, *118*, 364–374, doi:10.1029/2012JA018.065.
Phan, T. D., G. Paschmann, A. Raj, V. Angelopoulos, D. Larson, and R. P. Lin (1998), Wind observations of the halo/cold plasma sheet, in *Substorms-4*, edited by S. Kokubun and Y. Kamide, Terra Scientific/Kluwer Acad., Boston, Mass.
Quinn, J. M., and D. J. Southwood (1982), Observations of parallel ion energization in the equatorial region, *J. Geophys. Res.*, *87*, 10,536–10,540.
Raeder, J. (2003), Global magnetohydrodynamics: A tutorial, in *Space Plasma Simulation*, pp. 212–246, Springer, Berlin.
Raeder, J., R. J. Walker, and M. Ashour-Abdalla (1995), The structure of the distant geomagnetic tail during long periods of northward IMF, *Geophys. Res. Lett.*, *22*, 349–352.
Raeder, J., J. Berchem, M. Ashour-Abdalla, L. A. Frank, W. R. Paterson, K. L. Ackerson, R. P. Lepping, S. Kokubun, T. Yamamoto, and S. A. Slavin (1997), Boundary layer formation in the magnetotail: Geotail observations and comparisons with a global MHD model, *Geophys. Res. Lett.*, *24*, 951–954.
Raeder, J., J. Berchem, and M. Ashour-Abdalla (1998), The geospace environment modeling grand challenge: Results from a global geospace circulation model, *J. Geophys. Res.*, *103*, 14,787–14,798.
Raeder, J., R. L. McPherron, L. A. Frank, W. R. Paterson, J. B. Sigwarth, G. Lu, H. J. Singer, S. Kokubun, T. Mukai, and J. A. Slavin (2001), Global simulation of the geospace environment modeling substorm challenge event, *J. Geophys. Res.*, *106*, 381–395.
Raeder, J., D. Larson, W. Li, E. L. Kepko, and T. Fuller-Rowell (2008), OpenGGCM simulations for the THEMIS mission, *Space Sci. Rev.*, *141*, 535–555, doi:10.1007/s11214-008-9421-5.
Robinson, R. M., R. R. Vondrak, K. Miller, T. Dabbs, and D. Hardy (1987), On calculating ionospheric conductances from the flux and energy of precipitating electrons, *J. Geophys. Res.*, *92*, 2565–2569.
Sojka, J. J., and G. L. Wrenn (1985), Refilling of geosynchronous flux tubes as observed at the equator by GEOS 2, *J. Geophys. Res.*, *90*(A7), 6379–6385, doi:10.1029/JA090iA07p06.379.
Song, P., and C. T. Russell (1992), Model of the formation of the low-latitude boundary layer for strongly northward interplanetary magnetic field, *J. Geophys. Res.*, *97*, 1411–1420.
Song, P., D. L. DeZeeuw, T. I. Gombosi, C. P. T. Groth, and K. G. Powell (1999), A numerical study of solar wind-magnetosphere interaction for northward interplanetary magnetic field, *J. Geophys. Res.*, *104*, 28,361–28,378.
Sonnerup, B. U. O., and L. J. Cahill (1967), Magnetopause structure and attitude from Explorer 12 observations, *J. Geophys. Res.*, *72*, 171–183.
Sonnerup, B. U. O., and L. J. Cahill (1968), Explorer 12 observations of the magnetopause current layer, *J. Geophys. Res.*, *73*, 1757–1770.
Terasawa, T., M. Fujimoto, T. Mukai, I. Shinohara, Y. Saito, T. Yamamoto, S. Machida, S. Kokubun, A. J. Lazarus, and J. T. Steinberg (1997), Solar wind control of density and temperature in the near-Earth plasma sheet: WIND/GEOTAIL collaboration, *Geophys. Res. Lett.*, *24*, 935–938.
Thomsen, M. F., J. E. Borovsky, D. J. McComas, and M. R. Collier (1998), Variability of the ring current source population, *Geophys. Res. Lett.*, *25*, 3481–3484.
Thomsen, M. F., J. E. Borovsky, R. M. Skoug, and C. W. Smith (2003), Delivery of cold, dense plasma sheet material into the near-Earth region, *J. Geophys. Res.*, *108*, 1151, doi:10.1029/2002JA009.544.
Yau, A. W., E. G. Shelley, W. K. Peterson, and L. Lenchyshyn (1985), Energetic auroral and polar ion outflow at DE 1 altitudes: Magnitude, composition, magnetic activity dependence, and long-term variations, *J. Geophys. Res.*, *90*, 8417–8432.
Young, D. T., H. Balsiger, and J. Geiss (1982), Correlations of magnetospheric ion composition with geomagnetic and solar activity, *J. Geophys. Res.*, *87*(A11), 9077–9096, doi:10.1029/JA087iA11p09077.
Zhang, L. Q., J. Y. Wang, W. Baumjohann, H. Rème, L. Dai, M. W. Dunlop, T. Chen, and Y. Huang (2015), X lines in the magnetotail for southward and northward IMF conditions, *J. Geophys. Res. Space Physics*, *120*, 7764–7773, doi:10.1002/2015JA021503.
Zhang, Q.-H., M. Lockwood, J. C. Foster, S.-R. Zhang, B.-C. Zhang, I. W. McCrea, J. Moen, M. Lester, and J. M. Ruohoniemi (2015), Direct observations of the full Dungey convection cycle in the polar ionosphere for southward interplanetary magnetic field conditions, *J. Geophys. Res. Space Physics*, *120*, 4519–4530, doi:10.1002/2015JA021172.